The Astrophysical Journal, 876:128 (8pp), 2019 May 10 https://doi.org/10.3847/1538-4357/ab06c2

Radioactive Heating and Late Time Kilonova Light Curves

Daniel Kasen[1] and Jennifer Barnes[2,3]
[1] Departments of Physics and Astronomy, University of California Berkeley and Lawrence Berkeley National Laboratory, USA; kasen@berkeley.edu
[2] Columbia Astrophysics Laboratory, Columbia University, New York, NY 10025, USA; jlb2331@columbia.edu
Received 2018 July 9; revised 2019 January 25; accepted 2019 February 11; published 2019 May 10

Abstract

Compact object mergers can produce a thermal electromagnetic counterpart (a "kilonova") powered by the decay of freshly synthesized radioactive isotopes. The luminosity of kilonova light curves depends on the efficiency with which beta-decay electrons are thermalized in the ejecta. Here we derive a simple analytic solution for thermalization by calculating how accumulate electrons lose energy adiabatically and via plasma interactions. The thermalization efficiency is well described by $f(t) \approx (1 + t/t_e)^{-n}$ where the timescale t_e is a function of the ejecta mass and velocity and the exponent $n \approx 1.0$–1.5 depends on the electron energies and the thermalization cross-sections. For a statistical distribution of r-process isotopes with radioactive power $\dot{Q}_\beta \propto t^{-4/3}$ and $n = 1$, the late time kilonova luminosity asymptotes to $L = f(t)\dot{Q}_\beta \propto t^{-7/3}$ and depends super-linearly on the ejecta mass, $L \propto M^{5/3}$. If a kilonova is instead powered by a single dominate isotope, we show that the late time luminosity can deviate substantially from the underlying exponential decay and the heating from the accumulation of trapped electrons eventually exceeds the instantaneous radioactivity. Applied to the kilonova associated with the gravitational wave source GW170817, these results imply that a possible steepening of the light curve at $\gtrsim$7 days is unrelated to thermalization effects and instead could mark the onset of translucency in a high opacity component of ejecta. The analytic results should be convenient for estimating the properties of observed kilonovae and assessing the potential late time detectability of future events.

Key words: gravitational waves – nuclear reactions, nucleosynthesis, abundances – plasmas – stars: neutron

1. Introduction

The violent merger of two neutron stars (or a neutron star and a black hole) can eject neutron-rich matter that, upon decompression, will assemble into heavy nuclei via rapid neutron capture (the r-process; Lattimer & Schramm 1976; Eichler et al. 1989; Meyer 1989; Freiburghaus et al. 1999; Rosswog et al. 1999). The subsequent radioactive decay of these freshly made nuclei was predicted to power a thermal electromagnetic transient known as a kilonova (Li & Paczyński 1998; Metzger et al. 2010; Roberts et al. 2011; Barnes & Kasen 2013). Electromagnetic follow-up of the gravitational wave source GW170817 (Abbott et al. 2017a) appears to confirm the existence of an optical/infrared kilonova with properties in general agreement with theoretical expectations for a neutron star merger (e.g., Abbott et al. 2017b; Arcavi et al. 2017; Chornock et al. 2017; Coulter et al. 2017; Cowperthwaite et al. 2017; Drout et al. 2017; Kasen et al. 2017; Kasliwal et al. 2017; Kilpatrick et al. 2017; McCully et al. 2017; Nicholl et al. 2017; Shappee et al. 2017; Smartt et al. 2017; Soares-Santos et al. 2017; Tanaka et al. 2017; Tanvir et al. 2017)

Interpreting kilonova observations requires understanding the processes by which radioactive decay particles deposit energy (i.e., "thermalize") in the ejected material. Radioactivity produces energetic particles (photons, electrons, alphas, and fission fragments), which are only partially absorbed and reradiated as thermal light. The thermalization efficiency declines with time as the ejecta expand and dilute, which substantially influences the evolution of the kilonova light curve.

[3] NASA Einstein Fellow.

At early times, the luminosity of kilonovae is complicated by radiation transport effects related to the diffusion of thermal optical/infrared photons through the opaque ejecta. However, at later times ($\gtrsim$days to weeks), the ejecta become optically thin and the bolometric light curve directly tracks the instantaneous deposition of radioactive energy. This makes the late time light curves of kilonovae particularly sensitive probes of merger ejecta. A simple theoretical description of thermalization and emission at these phases would be useful for estimating the physical properties and detectability of kilonovae.

Metzger et al. (2010) made initial analytic estimates of the thermalization in kilonovae, while Hotokezaka et al. (2016) studied the absorption and potential detectability of r-process gamma-rays. Barnes et al. (2016) carried out detailed numerical calculations of thermalization efficiency for all r-process decay products, including electrons, alpha particles and fission fragments. Waxman et al. (2018) applied an analytic treatment of electron thermalization to model the kilonova that accompanied GW170817. The steep decline of the efficiency adopted by Waxman et al. (2018) is in tension with the more gradual decrease seen in the numerical results of Barnes et al. (2016), motivating a deeper analytic description of thermalization.

Here we derive analytic expressions for radioactive heating in kilonova that account for the several important physical processes at play. In particular, charged particles from decay are likely trapped by magnetic fields and accumulate locally until they are thermalized. The kilonova luminosity is then not simply a function of the instantaneous decay rate, but rather depends on the accumulated store of electrons emitted from prior epochs. We determine this cumulative heating by calculating how electrons deposit energy in the plasma while simultaneously losing energy due to adiabatic expansion.

Because plasma losses roughly follow the Bethe formula ($dE/dt \propto E^{-1/2} \ln E$), electrons deposit energy more effectively as they adiabatically degrade to lower energy E. We account for this energy dependence, along with the fact that in beta decay the longer lived nuclei on average emit lower-energy electrons.

The above physical processes were included in the detailed numerical thermalization calculations of Barnes et al. (2016). Here we show that, despite the apparent physical complexity, the essential behavior of radioactive heating can be well described by simple and intuitive analytic formulae. After a description of the decay and thermalization processes in kilonovae (Section 2), we derive solutions for the energy evolution and heating efficiency of suprathermal electrons in an expanding plasma (Section 3). The analytic results are then generalized to varying radioactivity decay parameters (Section 4) including heating dominated by a single isotope (Section 5). We provide convenient expressions for the thermalization timescale (Section 6) and the total (gamma-ray plus electron) thermalization efficiency of beta decay (Section 7). In Section 8 we summarize the most useful results, which are readily applicable to kilonova modeling, and discuss implications for the kilonova associated with GW170817.

2. Radioactive Heating in Kilonovae

The material ejected in compact object mergers is expected to consist of heavy neutron-rich isotopes that primarily undergo beta decay. If translead nuclei are present, alpha decay and fission may also contribute to the radioactivity. Detailed nuclear network calculations have shown that the radioactive power of r-process material is approximately described by a power law (e.g., Metzger et al. 2010; Roberts et al. 2011; Lippuner & Roberts 2015; Rosswog et al. 2018)

$$\dot{Q}_\beta(t) \approx 10^{10}\, t_{\rm d}^{-1.3}\ {\rm erg\ s^{-1}\ g^{-1}}, \tag{1}$$

where $t_{\rm d}$ is the time since merger measured in days.

The power-law dependence of $\dot{Q}_\beta(t)$ has been explained as follows. The r-process synthesizes a multitude of isotopes with a wide range of half-lives. Assuming that the decay times, $t_{\rm r}$, of isotopes are roughly equally distributed in log time (Li & Paczyński 1998) between $t_{\rm min} < t_{\rm r} < t_{\rm max}$, the integrated number of decays per unit time is

$$\dot{N}(t) \approx \frac{N}{\lambda_r}\int_{t_{\rm min}}^{t_{\rm max}} \frac{e^{-t/t_{\rm r}}}{t_{\rm r}} d(\ln t_{\rm r}) \approx \frac{N}{\lambda_r}\frac{e^{-t/t_{\rm max}}}{t}, \tag{2}$$

where N is the total number of isotopes, $\lambda_r = \ln(t_{\rm max}/t_{\rm min})$ is a normalization factor of the distribution, and we assumed $t \gg t_{\rm min}$. For times, $t_{\rm min} \ll t \ll t_{\rm max}$ the number of decays per unit time per gram is

$$\dot{n}(t) = \frac{\dot{N}(t)}{N\langle A\rangle m_p} = \left[\frac{1}{\langle A\rangle m_p \lambda_r}\right] t^{-1}, \tag{3}$$

where $\langle A\rangle$ is the mean atomic weight of isotopes and m_p is the proton mass.

The radioactive energy generation rate $\dot{Q}_\beta(t)$ declines more rapidly than $\dot{n}(t) \propto t^{-1}$ because longer lived isotopes typically have a lower-energy release (Colgate & White 1966; Metzger et al. 2010; Hotokezaka et al. 2016). From Fermi's theory of beta decay, the average energy released in a decay approximately follows $E_\beta \propto t_{\rm r}^{-a}$, where $a = 1/5$ in the relativistic beta-decay regime. For the epochs of interest to kilonovae (∼days), Hotokezaka et al. (2016) show that the nonrelativistic or nonrelativistic Coloumb regime applies, for which $a = 1/4$ and $a = 1/3$ respectively. Assuming that isotopes with half-lives $t_{\rm r} \approx t$ dominate at time t, the energy generation rate per gram is $\dot{Q}_\beta(t) = \dot{n}(t) E_\beta(t)$ or

$$\dot{Q}_\beta(t) \approx 10^{10}\frac{E_{\beta,d}}{m_e c^2}\frac{200}{\langle A\rangle} t_{\rm d}^{-(1+a)}\ {\rm erg\ s^{-1}\ g^{-1}}, \tag{4}$$

where $E_{\beta,d}$ is the average energy of a beta decay at 1 day. The analytic estimate resembles the numerical result Equation (1) with $a \approx 1/3$.

Beta decays produce gamma-rays, electrons, and neutrinos, only a fraction of which will be absorbed and reradiated as kilonova light. The neutrinos escape straightaway, while gamma-rays will only be effectively absorbed at early times (see Section 7). After a few days, the kilonova emission is powered mainly by electrons depositing energy through impact ionization and excitation of ambient atoms (Barnes et al. 2016). The ionization energy loss rate for nonthermal electrons (ignoring relativistic corrections) is given by the Bethe formula

$$\frac{dE_{\rm ion}t}{dt} = -\frac{\pi q_e^4}{m_e v_e} n_{\rm b} \ln\left(\frac{E}{\chi}\right), \tag{5}$$

where χ is the effective ionization potential, n_b is the number density of bound electrons, and q_e, v_e, E are the electron charge, velocity, and energy, respectively. For nonrelativistic electrons, the loss rate scales as $E^{-1/2}\ln(E)$, i.e., lower-energy electrons thermalize more readily. Plasma loss due to interactions with free electrons has a similar functional form but is expected to be subdominant given the low-ionization state of kilonova ejecta.

Beta-decay electrons also lose energy as they do work on the expanding ejecta. For kilonovae, the ejecta velocity structure rapidly becomes homologous (velocity proportional to radius) and the ejecta volume increases as $V \propto t^3$. The energy loss to adiabatic expansion is then

$$\frac{dE_{\rm ad}}{dt} = -x\frac{E}{t}, \tag{6}$$

where $x = 2$ for nonrelativistic and $x = 1$ for relativistic particles. For purely adiabatic evolution the electron energy follows $E \propto t^{-x}$. The energy lost to expansion goes into increasing the ejecta kinetic energy and is not available to power the kilonova luminosity. A complete treatment of the electron heating efficiency must therefore account for both adiabatic and ionization loses.

The propagation of electrons through the kilonova ejecta is hindered by magnetic fields. The fields initially present in the neutron star merger will be diluted by ejecta expansion, but the expected residual field strength ($B \sim \mu$g) still implies an electron Larmor radius $\sim 10^6$ times smaller than the ejecta size (Barnes et al. 2016). Assuming magnetic fields are not ordered on large scales, electrons are effectively trapped at a specific mass coordinate and advected with the fluid flow.

3. Analytic Expression for Thermalization

We now derive analytic formulae for the thermalization efficiency of electrons (or other charged particles) in a homologously expanding medium. We assume electrons are

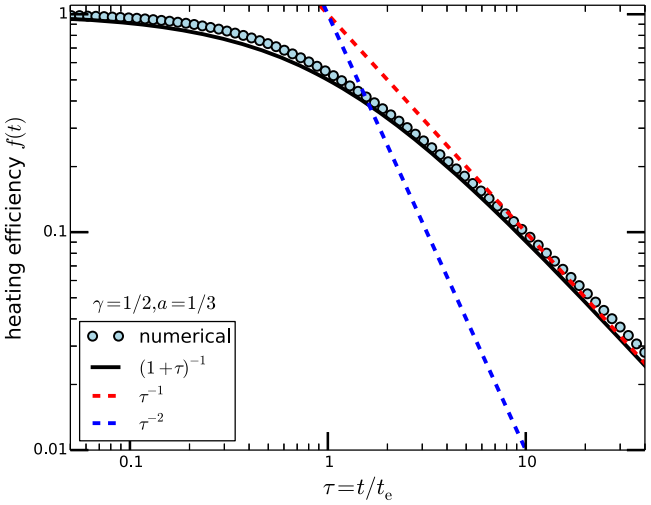

Figure 1. Thermalization efficiency of electrons as a function of time for standard parameters. The numerical result is derived from integrating the plasma loses of accumulated electrons subject to adiabatic loses. The analytic interpolation formula Equation (22) $f(\tau) = (1+\tau)^{-1}$ well approximates the numerical solution, which approaches $f(\tau) \propto \tau^{-1}$ at late times. This calculation uses parameters $\gamma = 1/2$, $b = 1$, $a = 1/3$, $x = 2$.

trapped locally by magnetic fields at a fixed Lagriangian coordinate, where the time-dependent density is

$$\rho(t) = \frac{3M_{\rm ej}}{4\pi v_{\rm max}^3 t^3}\eta, \tag{7}$$

where $M_{\rm ej}$ is the ejecta mass, $v_{\rm max}$ the maximum ejecta velocity, and η is a dimensionless parameter that depends on the density structure (for a uniform spherical distribution, $\eta = 1$). The corresponding number density of bound electrons is $n_b(t) = \rho(t)\langle Z\rangle/\langle A\rangle m_p$, where $\langle Z\rangle$ and $\langle A\rangle$ are the average nuclear charge and weight, respectively, of isotopes, which are expected to be in a low-ionization state.

The total energy loss rate of a nonrelativistic electron, including both adiabatic (Equation (6) with $x = 2$) and ionization (Equation (5)) losses is

$$\frac{dE}{dt} = -2\frac{E}{t} - \frac{\pi q_e^4}{m_e v_e}\frac{3M_{\rm ej}\eta}{4\pi v_{\rm max}^3 t^3}\frac{\langle Z\rangle}{\langle A\rangle}\frac{\lambda_\chi}{m_p}, \tag{8}$$

where $\lambda_\chi = \ln(E/\chi)$. For the moment we take λ_χ to be constant, but in Section 4 will adopt a more general dependence of the ionization losses. Defining a characteristic thermalization timescale

$$t_{\rm e} = \frac{1}{E_\tau^{3/4}}\left[\frac{3}{\sqrt{32}}\frac{q_e^4\lambda_\chi}{m_e^{1/2}m_p}\frac{M_{\rm ej}\eta}{v_{\rm max}^3}\frac{\langle Z\rangle}{\langle A\rangle}\right]^{1/2}, \tag{9}$$

we write the energy evolution equation in dimensionless form

$$\frac{d\epsilon}{d\tau} = -\frac{2\epsilon}{\tau} - \frac{\epsilon^{-1/2}}{\tau^3}, \tag{10}$$

where $\tau = t/t_{\rm e}$ and $\epsilon = E/E_\tau$. Here E_τ is the average energy of electrons emitted at scaled time $\tau = 1$. The value of $t_{\rm e}$ sets the timescale at which electron thermalization begins to become inefficient; we will give convenient expressions for calculating it in Section 6.

Solving the differential equation Equation (10) we find the evolution of an electron's energy

$$\epsilon(\tau, \tau_0) = \epsilon_0\left(\frac{\tau_0}{\tau}\right)^2\left[1 - \frac{3}{2}\frac{\epsilon_0^{-3/2}}{\tau_0^3}(\tau - \tau_0)\right]^{2/3}, \tag{11}$$

where ϵ_0 is the initial energy of an electron emitted at time τ_0. We assume now that the electrons emitted at τ_0 come primarily from beta decays with decay times $t_{\rm r}/t_e \approx \tau_0$. Following the discussion of beta decay in Section 2 we write $\epsilon_0 = \tau_0^{-a}$, which gives

$$\epsilon(\tau, \tau_0) = \tau_0^{-a}\left(\frac{\tau_0}{\tau}\right)^2\left[1 - \frac{3}{2}\left(\frac{\tau - \tau_0}{\tau_0^{3-3a/2}}\right)\right]^{2/3}. \tag{12}$$

For specificity, we adopt $a = 1/3$ in what follows but generalize to arbitrary values in Section 4.

At any given time, the ejecta is heated by the cumulative deposition from electrons emitted at earlier times. The oldest electrons still in existence at a time τ are those emitted at a time τ_1 such that $\epsilon(\tau, \tau_1) = 0$, which is satisfied when

$$\tau_1 + \frac{2}{3}\tau_1^{5/2} = \tau. \tag{13}$$

The equation is not readily solvable for τ_1 but the limiting cases can be determined. For $\tau_1 \ll 1$ particles thermalize nearly instantaneously, $\tau_1 \approx \tau$. For $\tau_1 \gg 1$ thermalization is inefficient and

$$\tau_1 \approx \left(\frac{3}{2}\tau\right)^{2/5} \quad \text{for } \tau_1 \gg 1. \tag{14}$$

To derive the instantaneous heating rate per gram, $\dot{q}_{\rm dep}(\tau)$, we integrate the plasma losses (Equation (5)) of all existing electrons produced between times τ_1 and τ

$$\dot{q}_{\rm dep}(\tau) = E_\tau\int_{\tau_1}^{\tau}\dot{n}(\tau_0)\frac{[\epsilon(\tau, \tau_0)]^{-1/2}}{\tau^3}d\tau_0. \tag{15}$$

The factor of E_τ is included so that $\dot{q}_{\rm dep}(\tau)$ has physical units of energy. Here $\dot{n}(t)$ is the number of electrons emitted per unit time per gram, which is taken from Equation (3), giving

$$\dot{q}_{\rm dep}(\tau) = \frac{E_\tau}{\langle A\rangle m_p\lambda_r t_{\rm e}}\int_{\tau_1}^{\tau}\frac{[\epsilon(\tau, \tau_0)]^{-1/2}}{\tau_0\tau^3}d\tau_0 \tag{16}$$

and $\epsilon(\tau, \tau_0)$ is given by Equation (12). The integration must be done numerically in general, but we can determine the behavior in the asymptotic limit $\tau \gg 1$. Since thermalization is inefficient at these times, the energy of particles degrades primarily adiabatically ($\epsilon \propto \tau^{-2}$) and we approximate

$$\epsilon(\tau, \tau_0) \approx \tau_0^{-1/3}(\tau_0/\tau)^2. \tag{17}$$

Integration of Equation (16) then gives the asymptotic heating rate

$$\dot{q}_{\rm a}(\tau) \approx \frac{6}{5}\frac{E_\tau}{\langle A\rangle m_p\lambda_r t_{\rm e}}\frac{1}{\tau^2}[\tau_1^{-5/6} - \tau^{-5/6}]. \tag{18}$$

Working in the limit of weak thermalization, $\tau_1 \ll \tau$, we neglect the second term in brackets and use the limiting value

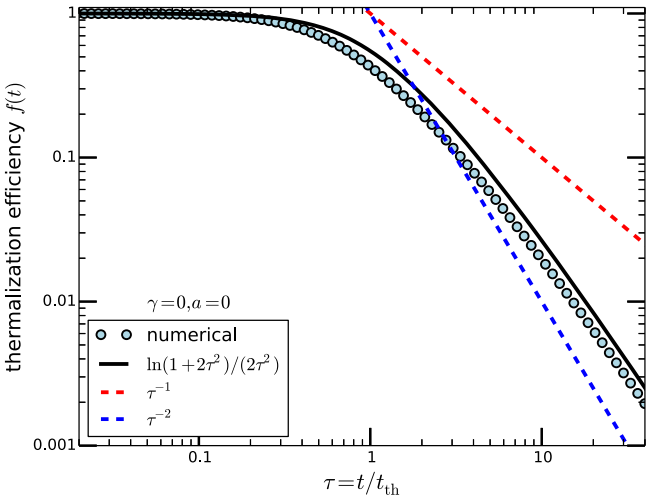

Figure 2. Thermalization efficiency of electrons as a function of time for the case $a = 0$, $\gamma = 0$ (i.e., all electrons emitted with the same energy and plasma loses independent of particle energy). The analytic interpolation formula Equation (31) reasonably approximates the numerical solution, which declines as $f(\tau) \propto \tau^{-0.8}$ at $\tau \approx 1$ and gradually steepens to $f(\tau) \propto \tau^{-1.6}$ at $\tau \approx 10$. This calculation uses parameters $\gamma = 0$, $b = 1$, $a = 0$, $x = 2$.

of $\tau_{\rm l}$ (Equation (14)) to find

$$\dot{q}_{\rm a}(\tau) \approx \left(\frac{144}{125}\right)^{1/3}\left(\frac{E_\tau}{\bar{A} m_p \lambda_r t_{\rm e}}\right)\tau^{-7/3}. \quad (19)$$

The electron thermalization efficiency is defined as $f(\tau) = \dot{q}_{\rm dep}(\tau)/\dot{Q}_e(\tau)$, where $\dot{Q}_e(\tau)$ is the instantaneous radioactive energy generation rate of electrons (i.e., that fraction of the total beta-decay power $\dot{Q}_\beta$ emitted in the form of electrons)

$$\dot{Q}_e(\tau) = \dot{n}(\tau) E_\tau \tau^{-1/3} = \frac{E_\tau}{\langle A\rangle m_p \lambda_r t_{\rm e}}\tau^{-4/3}. \quad (20)$$

Dividing Equation (19) by Equation (20) we find the asymptotic thermalization efficiency

$$f_{\rm a}(\tau) \approx \left(\frac{144}{125}\right)^{1/3}\tau^{-1}. \quad (21)$$

The coefficient is close to unity, so we arrive at the simple result $f_{\rm a}(\tau) \approx \tau^{-1}$.

The analytic solution Equation (21) applies only at late times ($\tau \gg 1$). At early times ($\tau \ll 1$) particles thermalize efficiently and $f(\tau) \to 1$. An ad hoc formula that interpolates between the two limits is

$$f(\tau) \approx (1 + \tau)^{-1}. \quad (22)$$

Figure 1 shows $f(\tau)$ calculated by numerical integration of Equation (16) using the full electron energy dependence (Equation (12)). The asymptotic behavior approaches the analytic result $f(\tau) \propto \tau^{-1}$. The simple analytic interpolation formula Equation (22) reproduces the numerical solution at all epochs to better than 10%.

The efficiency only gradually approaches the asymptotic behavior $f(\tau) \propto \tau^{-1}$. To quantify the time dependence at any instant we can write $f(\tau) \propto \tau^{-n_{\rm eff}(\tau)}$, where the effective exponent

$$n_{\rm eff}(\tau) \approx -\frac{\partial(\log f)}{\partial(\log \tau)} \approx \frac{1}{1+\tau} \quad (23)$$

and so $n_{\rm eff} \leqslant 1$ for all τ. In particular, at the onset of inefficient thermalization ($\tau = 1$), the decline rate is only half of the asymptotic result, $n_{\rm eff} = 0.5$. This behavior is noticeable in tabulated fits to numerical calculations (Barnes et al. 2016), where $n_{\rm eff}$ is smaller for models with greater t_e (i.e., larger $M_{\rm ej}$ or smaller $v_{\rm max}$).

4. Generalized Solution

The above thermalization calculation adopted specific dependencies for the electron generation rate, initial electron energies, and the plasma loss rate. We now derive a more general solution. We write the number of electrons generated per gram per unit time as

$$\dot{n} = B\tau^{-b}, \quad (24)$$

where B and b are constants. We take the initial energy of electrons emitted to be $\epsilon(\tau_0) = \tau_0^{-a}$ and generalize the electron energy equation (Equation (10)) to

$$\frac{d\epsilon}{d\tau} = -x\frac{\epsilon}{\tau} - \frac{\epsilon^{-\gamma}}{\tau^3}, \quad (25)$$

where $x = 1$–2 quantifies how relativistic the electrons are and γ describes the energy dependence of loses to the plasma.

In Section 3 we adopted default values $a = 1/3$, $b = 1$, $x = 2$, $\gamma = 1/2$. The actual values likely differ only modestly. The energy dependence of ionization losses may be weaker than $\gamma = 1/2$ due to the $\lambda_\chi = \log(E_e/\chi)$ term in Equation (5) and relativistic corrections. Inspecting Equation (5) we find that $\gamma \approx 1/4 - 1/2$ over the energy range of interest.

Calculation of the asymptotic thermalization efficiency in the more general formulation can be carried out in the way described in Section 3. We find $f_{\rm a}(t) \approx \tau^{-n}$, where

$$n = 1 - a + \frac{1-\gamma}{1+\gamma} - (b-1)\frac{(2 - a - a\gamma)}{(x-a)(1+\gamma)}. \quad (26)$$

This solution assumes $b + (x - a)\gamma > 1$ and $\gamma > 0$. As before, we introduce an ad hoc interpolation between the limiting behaviors

$$f(\tau) = (1 + \tau)^{-n}. \quad (27)$$

For parameters that do not differ much from the defaults, n deviates only modestly from unity. For example, for $b = 1$, $a = 1/3$, $x = 2$ we find $n = 1.166$ for $\gamma = 1/3$ and $n = 1.266$ for $\gamma = 1/4$.

In the limit $\gamma \to 0$, the approximations applied in the above derivation break down. As an example of the behavior in this regime, we consider the specific case $\gamma = 0$, $b = 1$ where integration of the heating gives

$$\dot{q}_{\rm dep}(\tau) = \frac{E_\tau}{\langle A\rangle m_p \lambda_r t_{\rm e}}\frac{\ln(\tau/\tau_{\rm l})}{\tau^{3-a}}. \quad (28)$$

An expression for $\tau_{\rm l}$ can be determined by solving the energy equation, Equation (10),

$$\ln\tau = \ln\tau_{\rm l} + \tau_{\rm l}^2. \quad (29)$$

Calculation of $\tau_{\rm l}$ must be done numerically, but at late times we have $\tau = \tau_{\rm l} e^{\tau_{\rm l}^2} \gg \tau_{\rm l}$ and so the asymptotic heating efficiency is

$$f_a(\tau) \approx \frac{\ln(\tau)}{\tau^{2-a}} \quad (\text{for } \gamma = 0,\ b = 1). \quad (30)$$

For $a = 0$, this efficiency decays more slowly by a factor of $\ln(\tau)$ than the $f_a(\tau) \propto \tau^{-2}$ implied by Equation (26) and adopted by Waxman et al. (2018). This logarithmic factor was found in the analytic derivation of Barnes et al. (2016), which carried out a similar integration over trapped electrons. The analytics of Barnes et al. (2016) neglected adiabatic losses, but these do not affect the limiting functional form.

To describe the full time dependence of $f(\tau)$ in the limit $\gamma = 0$ we can use an interpolation formula motivated by the analytic result of Barnes et al. (2016)

$$f(\tau) \approx \frac{\ln(1 + 2\tau^{2-a})}{2\tau^{2-a}} \quad (\text{for } \gamma = 0,\ b = 1), \tag{31}$$

Figure 2 shows that it provides a reasonable fit to the true numerical solution for these parameters.

The decay rate at any instant in time can be quantified as $f(\tau) \propto \tau^{-n_{\rm eff}(\tau)}$ with (for $a = 0$)

$$n_{\rm eff}(\tau) \approx -\frac{\partial(\log f)}{\partial(\log \tau)} = 2 - \frac{1}{\ln(1 + 2\tau^2)} \frac{4\tau^2}{1 + 2\tau^2}, \tag{32}$$

which shows that when inefficiency begins to set in ($\tau = 1$) $n_{\rm eff} \approx 0.8$ which steepens to $n_{\rm eff} \approx 1.6$ at very late times $\tau \approx 10$.

5. Single Isotope Heating

For some r-process compositions, deviations from a power-law decay rate $\dot{n} \propto t^{-1}$ can occur at times $t > t_{\rm max}$, when the statistical distribution of isotopes cuts off and individual species begin to dominate the radioactive power. We therefore adapt the previous analysis to derive the heating rate from the exponential decay of a single isotope of decay times $t_{\rm r}$. The number of decays per unit time per gram is now

$$\dot{n}_i(t) = \frac{X_i}{A m_p t_{\rm r}} e^{-t/t_{\rm r}}, \tag{33}$$

where A is the atomic mass number and X_i is the mass fraction of the isotope. The instantaneous radioactive power is $Q_i(t) = E_i \dot{n}_i(t)$ where the energy released per decay E_i is constant with time (i.e., $a = 0$). The integral for the heating rate (Equation (15)) becomes for this single isotope case

$$q_i(\tau) = \frac{X_i E_i}{A m_p t_{\rm r}} \int_{\tau_1}^{\tau} e^{-\tau_0 \frac{t_{\rm e}}{t_{\rm r}}} \frac{[\epsilon(\tau, \tau_0)]^{-1/2}}{\tau^3} d\tau_0, \tag{34}$$

where we have adopted an energy loss dependence $\gamma = 1/2$. The emission time, τ_1, of the oldest living electrons can be determined from electron energy evolution Equation (12) with $a = 0$

$$\frac{2}{3}\tau_1^3 + \tau_1 = \tau \tag{35}$$

and so $\tau_1 = \sqrt[3]{3\tau/2}$ for $\tau_1 \gg 1$.

As before, we approximate the late time energy evolution by the adiabatic formula, $\epsilon(\tau, \tau_0) \approx \tau_0^2/\tau^2$, and integrate Equation (34) to find

$$q_i(\tau) = \frac{X_i E_i}{A m_p t_{\rm r}} \frac{1}{\tau^2} [\mathcal{E}_i(\tau t_{\rm e}/t_{\rm r}) - \mathcal{E}_i(\tau_1 t_{\rm e}/t_{\rm r})], \tag{36}$$

where $\mathcal{E}_i$ is the exponential integral. In the weak thermalization limit we can neglect the first term in brackets and use the limiting behavior of the exponential integral $\mathcal{E}_i(x) \approx -e^{-x}/x$, to derive the asymptotic heating rate

$$q_{i,a}(\tau) = \frac{X_i E_i}{A m_p t_{\rm e}} \left(\frac{2}{3}\right)^{1/3} \frac{\exp[-\sqrt[3]{3\tau/2}\,(t_{\rm e}/t_{\rm r})]}{\tau^{7/3}}. \tag{37}$$

The asymptotic thermalization efficiency $f_{i,a}(\tau) = q_{i,a}(\tau)/Q_i(\tau)$ for a single isotope is

$$f_{i,a}(\tau) = \frac{t_{\rm r}}{t_{\rm e}} \left(\frac{2}{3}\right)^{1/3} \frac{\exp[t_e/t_{\rm r}(\tau - \sqrt[3]{3\tau/2})]}{\tau^{7/3}}, \tag{38}$$

which has the interesting behavior that the efficiency, at some point, increases with time and eventually will exceed unity. Though perhaps unexpected, $f(\tau) > 1$ is possible when the heating from accumulated electrons emitted from previous epochs dominates over the instantaneous generation rate. This is realized for the steep exponential decay rate of a single isotope, as well as for power-law decay rates when the exponent b is large enough to give $n < 0$ in Equation (26).

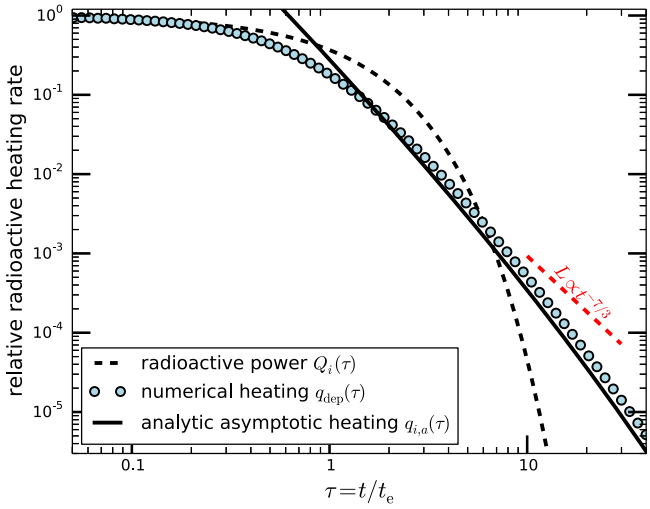

Figure 3. Radioactive heating (relative to the value at $t = 0$) for a kilonova powered by a single isotope with a half life taken to be equal to the electron thermalization time $t_{\rm e}$. The heating rate q_i (filled circles) deviates substantially from the underlying radioactive decay power $Q_i \propto e^{-t/t_{\rm r}}$ (dashed black line). At late times ($\tau \gtrsim 7$) the heating due to electrons accumulated from early epochs exceeds the instantaneous generation rate Q_i, such that the thermalization efficiency is formally greater than one. The analytic formula Equation (37) (solid black line) reasonably approximates the later time ($\tau \gtrsim 1$) behavior.

Figure 3 shows a numerical integration of the radioactive heating from a single isotope with $t_{\rm r} = t_e$. Initially $f(\tau) < 1$, but eventually the integrated heating due to electrons from earlier epochs exceeds the instantaneous radioactive power and $f(\tau)$ becomes formally greater than one. The radioactive heating rate differs substantially from the underlying exponential decay $\propto e^{-t/t_{\rm r}}$, and is reasonably approximated at times $\tau \gtrsim 1$ by the analytic result Equation (37). Comparing this single isotope heating to that of a statistical distribution (Equation (19)) we see both share a $\tau^{-7/3}$ dependence, though the single isotope case declines more steeply due to the exponential factor in Equation (37).

6. Thermalization Timescale

In our formalism, electron thermalization depends on a single dimensional parameter, t_e, which sets the timescale over which thermalization becomes inefficient. We defined t_e in

Equation (9) as a function of E_τ, the energy of electrons emitted at time $t = t_e$. It is convenient to rewrite t_e in terms of the energy of electrons emitted at some fixed time, say $t = 1$ day after merger. Using the time dependence of the electron energy, $E(\tau) = E_\tau \tau^{-a}$ we rewrite t_e from Equation (9) as

$$t_{\rm e} = \left[\frac{E_{\rm day}}{m_e c^2}\left(\frac{t_{\rm e}}{1\ {\rm day}}\right)^{-a}\right]^{-3/4} t_{\rm e,0}, \tag{39}$$

where $E_{\rm day}$ is the energy of electrons emitted at 1 day and

$$t_{\rm e,0} = \left[\frac{3}{\sqrt{32}}\frac{q_e^4 \lambda_\chi}{m_e^2 m_p c^3}\frac{M\eta}{v_{\rm max}^3}\frac{\bar{Z}}{\bar{A}}\right]^{1/2} \tag{40}$$

is the thermalization timescale of an electron emitted with energy $m_e c^2$. Solving Equation (39) for t_e gives the desired expression for t_e

$$t_{\rm e} = \left(\frac{E_{\rm day}}{m_e c^2}\right)^{-3/(4-3a)}\left(\frac{t_{\rm e,0}}{1\ {\rm day}}\right)^{4/(4-3a)} {\rm days}. \tag{41}$$

To get a sense of the timescales involved, we scale to values typical for kilonovae. For the case $a = 0$ we have

$$t_{\rm e} = 6.8\, M_{0.01}^{1/2} v_{0.2}^{-3/2} \zeta^{1/2}\ {\rm days} \quad (a = 0), \tag{42}$$

where $M_{0.01} = M_{\rm ej}/10^{-2} M_\odot$ and $v_{0.2} = v_{\rm max}/0.2c$. For the case $a = 1/3$ (our fiducial choice)

$$t_{\rm e} \approx 12.9\, M_{0.01}^{2/3} v_{0.2}^{-2} \zeta^{2/3}\ {\rm days} \quad (a = 1/3), \tag{43}$$

above we have introduced for convenience the variable

$$\zeta = \eta\left(\frac{\lambda_\chi}{10}\right)\frac{2\langle Z\rangle}{\langle A\rangle}\left(\frac{E_{\rm day}}{m_e c^2}\right)^{-3/2}, \tag{44}$$

which is defined such that $\zeta \sim 1$ for typical values.

7. Total Thermalization Efficiency

In addition to electrons, beta-decay energy also emerges as gamma-rays and neutrinos. The neutrinos never thermalize, but gamma-ray deposition can be significant at early times (∼days). If a fraction p_γ of the energy emerges in gamma-rays and p_e in electrons, the total thermalization efficiency of beta decay is

$$f_\beta(t) = p_\gamma f_\gamma(t) + p_e f(t), \tag{45}$$

where $f_\gamma(t)$ is the thermalization efficiency of gamma-rays. Typical fractions for beta decay are $p_e = 0.2$, $p_\gamma = 0.5$ with the remaining $p_\nu = 0.3$ emerging as neutrinos (see Barnes et al. 2016; Hotokezaka et al. 2016).

Gamma-ray thermalization occurs primarily through inelastic Compton scattering off of bound electrons. The probability that a gamma-ray emitted at a velocity coordinate v is absorbed in the ejecta is $e^{-\tau(v)}$, where the radial optical depth from v to the surface is, for constant density ejecta

$$\tau(v) = \rho\kappa_\gamma(v_{\rm max} - v)t, \tag{46}$$

where κ_γ is the effective absorptive opacity which for ∼MeV gamma-rays is approximately $\kappa_\gamma = 0.06\, Y_e\ {\rm cm^2\ g^{-1}}$ (Swartz et al. 1995). The volume averaged optical depth is

$$\bar{\tau}_\gamma = \frac{3}{4\pi v_{\rm max}^3}\int_0^{v_{\rm max}} \tau(v) 4\pi v^2 dv = \frac{3\kappa_\gamma M}{16\pi v_{\rm max}^2 t^2}. \tag{47}$$

Averaging over nonradial gamma-ray trajectories only introduces a small (∼10%) correction.

The gamma-ray thermalization efficiency can then be written (Barnes et al. 2016; Hotokezaka et al. 2016)

$$f_\gamma(t) = 1 - \exp\left[-\frac{t_\gamma^2}{t^2}\right], \tag{48}$$

where t_γ is the timescale at which gamma-rays begin to thermalize inefficiently. For constant density ejecta

$$t_\gamma = \left(\frac{3M\kappa_\gamma}{16\pi v_{\rm max}^2}\right)^{1/2} \approx 0.3\, M_{0.01}^{1/2} v_{0.2}^{-1} \kappa_{\gamma,0.02}^{1/2}\ {\rm days}, \tag{49}$$

where $\kappa_{\gamma,0.02} = \kappa_\gamma/0.02\ {\rm cm^2\ g^{-1}}$.

In outflows with low electron fraction ($Y_e \lesssim 0.15$) the r-process can also synthesize significant quantities of translead nuclei (e.g., Mendoza-Temis et al. 2015) and alpha decay will contribute to the radioactive power. The total heating rate is then

$$\dot{q}_{\rm tot}(t) = f_\beta(t)\dot{Q}_\beta(t) + f_\alpha(t)\dot{Q}_\alpha(t), \tag{50}$$

where $\dot{Q}_\alpha$ and f_α are the radioactive power and thermalization efficiency of alpha decay. For low Y_e outflows, $\dot{Q}_\alpha$ may be from 5% to 40% of $\dot{Q}_\beta$ depending on what nuclear mass model is used. If many alpha-decaying isotopes are present, the statistical distribution of half-lives should mimic that of the beta-decaying nuclei and decline as a power-law $\dot{Q}_\alpha(t) \propto t^{-1}$. If instead the alpha decay is dominated by just a few isotopes, $\dot{Q}_\alpha(t)$ will more closely resemble an exponential.

The analytic formulae for thermalization (Section 4) can also be applied to alpha decay, for which $x = 2$ and $a = 0$. The plasma energy loss rate of alpha decay follows a rough power law with $\gamma = 0.3$ in the energy range of interest (Barnes et al. 2016). The thermalization efficiency is then described by $f_\alpha(\tau) \approx (1 + t/t_\alpha)^{-n}$ with $n \approx 1.5$, and where the thermalization timescale of alpha decay is roughly $t_\alpha \approx 3t_{\rm e}$, due to a higher plasma loss rate. In addition, the alpha-decay thermalization efficiency is enhanced relative to beta decays because no alpha-decay energy is lost to neutrinos or weakly thermalizing gamma-rays.

8. Discussion and Conclusion

We have derived simple but effective analytic formulae for calculating the radioactive heating in kilonovae. The fraction of beta-decay energy that is absorbed in the ejecta can be estimated using

$$f_\beta(t) = p_e\left(1 + \frac{t}{t_{\rm e}}\right)^{-n} + p_\gamma(1 - e^{-t_\gamma^2/t^2}), \tag{51}$$

with $n \approx 1$, and where $p_e \approx 0.2$, $p_\gamma \approx 0.5$ are the fractions of beta-decay energy emerging in electrons and gamma-rays, respectively. The thermalization timescales depend on ejecta mass and velocity as

$$t_{\rm e} \approx 12.9\, M_{0.01}^{2/3} v_{0.2}^{-2} \zeta^{2/3}\ {\rm days} \tag{52}$$

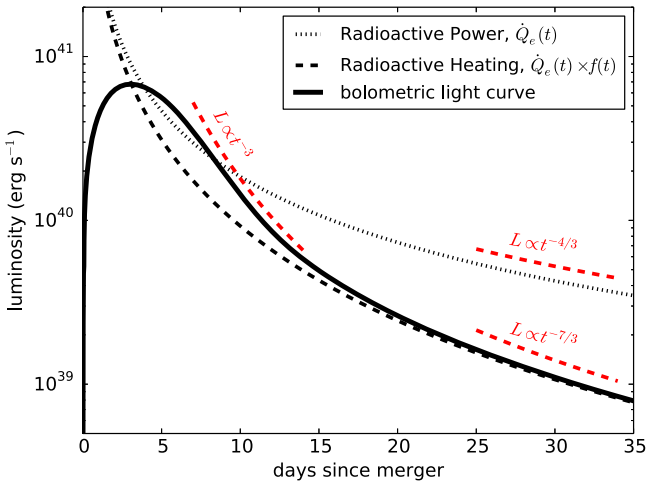

Figure 4. Toy analytic light curve of a kilonovae with radioactive power $Q_\beta \propto t^{-4/3}$ and a heating efficiency $f(t) = (1 + t/t_e)^{-1}$ with $t_e = 10$ days. The light curve is calculated using a simple Arnett-like one-zone semianalytic model (Arnett 1982; Kasen & Bildsten 2010) with an effective diffusion time, $t_d = 5$ days. The relatively steep decline $L \propto t^{-3}$ after peak is due to opacity effects as trapped radiation diffuses out of the ejecta, while the shallower late time decline follows the asymptotic result $L \propto t^{-7/3}$.

$$t_\gamma \approx 0.3\, M_{0.01}^{1/2} v_{0.2}^{-1} \text{ days}, \tag{53}$$

where $M_{0.01} = M_{\rm ej}/0.01\, M_\odot$, $v_{0.2} = v_{\rm max}/0.2c$, and $\zeta \sim 1$ is given by Equation (44). The summary equations above adopt several default assumptions regarding the radioactive decay behavior; more general results can be found in Section 4. In particular, for heating powered by a single isotope the late time efficiency is given by Equation (38)

Our analytic solutions permit simple estimates of the luminosity of a kilonova at later times. Once the ejecta have become optically thin to photons, the bolometric luminosity should track the instantaneous energy-deposition rate, $L_{\rm bol}(t) \approx M_{\rm ej} \dot{Q}_\beta(t) f_\beta(t)$, where the radioactive power of a statistical distribution of isotopes is

$$\dot{Q}_\beta(t) \approx 10^{10}\, \dot{\epsilon}_{10} t_{\rm d}^{-\alpha} \text{ erg s}^{-1} \text{ g}^{-1}, \tag{54}$$

where $\dot{\epsilon}_{10}$ is the radioactive energy generation rate at $t = 1$ day in units of 10^{10} ergs s^{-1} g^{-1}. Nuclear reaction networks find $\alpha \approx 4/3$ and $\dot{\epsilon}_{10} \approx 0.5$–$2.5$, with a relatively weak dependence on the ejecta conditions as long as they are sufficiently neutron rich (electron fraction $Y_e \lesssim 0.4$). If electrons dominate the heating at these epochs, the predicted bolometric luminosity is (using $p_e = 0.2$)

$$L_{\rm bol} \approx 4 \times 10^{40} \frac{\dot{\epsilon}_{10} M_{0.01} t_d^{-\alpha}}{(1 + 0.08 t_d M_{0.01}^{-2/3} v_{0.2}^2)^n} \text{ erg s}^{-1}. \tag{55}$$

At times late enough that the ejecta are both optically thin and inefficient at thermalizing electrons ($t \gg t_e$) the bolometric luminosity of Equation (55) becomes

$$L_{\rm bol} \approx 5.2 \times 10^{41}\, \dot{\epsilon}_{10} M_{0.01}^{5/3} v_{0.2}^{-2} t_d^{-(n+\alpha)} \text{ erg s}^{-1}. \tag{56}$$

The late time luminosity depends super-linearly on $M_{\rm ej}$, as a larger ejecta mass produces both greater radioactive power and a higher thermalization efficiency. For typical values $\alpha \approx 4/3$, $n \approx 1$ the asymptotic dependence is $L_{\rm bol}(t) \propto t^{-7/3}$.

We further derived analytic heating rates for radioactivity dominated by a single isotope with an exponential, rather than power-law, time dependence. This can occur for mildly neutron-rich outflows that synthesize only a narrow distribution of isotopes. Interestingly, the late time bolometric luminosity in this case eventually exceeds the instantaneous radioactive power (i.e., $f(t) > 1$). This is because the heating from electrons accumulated from earlier epochs eventually exceeds the generation rate of new electrons. The predicted late time light curves of single isotope kilonovae also have a $L_{\rm bol}(t) \propto t^{-7/3}$ dependence (Equation (37)) but modulated by an exponential factor that gives a steeper decline. The nontrivial behavior of $f(t)$ highlights the importance of carefully considering thermalization effects when trying to infer the radioactive source from late time bolometric measurements of kilonovae and supernovae.

We can apply our analytic results to the kilonova AT2017gfo associated with the neutron star merger GW170817. The bolometric luminosity at $t = 10$ days was $L_{\rm bol} \approx 10^{40}$ erg s^{-1}. Taking $\dot{\epsilon}_{10} = 1$, $\alpha = 4/3$, and $v_{\rm max} = 0.2\, c$, Equation (55) gives $M_{\rm ej} \approx 0.06\, M_\odot$, similar to estimates derived from more detailed modeling of the light curve. Uncertainties in the bolometric correction to the observations, along with the ejecta velocity, density profile, and nuclear heating rate $\dot{\epsilon}_{10}$, however, could introduce errors in $M_{\rm ej}$ at the factor of $\sim$2 level.

The time evolution of $f(t)$ is important for interpreting the bolometric light curve of AT2017gfo, which initially declined as $L_{\rm bol} \propto t^{-1}$ then appeared to steepen to $L_{\rm bol} \propto t^{-3}$ at times $t \gtrsim 7$ days (Cowperthwaite et al. 2017; Drout et al. 2017; Kasliwal et al. 2017; Kilpatrick et al. 2017; Smartt et al. 2017; Arcavi 2018; Coughlin & Dietrich 2018; Waxman et al. 2018). While this steepening has potentially interesting implications for the kilonova properties, it may also be an artifact of a shifting bolometric correction—late time observations are available in only a few wavelength bands and different published bolometric reconstructions find discrepant results (Arcavi 2018).

Waxman et al. (2018) ascribe the bolometric steepening in AT2017gfo to the onset of inefficient thermalization, which they model as a sudden transition from unity to $f(t) = (t/t_e)^{-2}$ for $t > t_e$. Our analysis indicates that this interpretation is unlikely—the thermalization efficiency has a weaker asymptotic decline $f(t) = (t/t_e)^{-1}$ and this is only approached gradually. At the onset of inefficiency ($t \approx t_e$, expected to occur $\sim$ weeks after the merger) the dependence is approximately $f(t) \propto t^{-0.5}$ (see Equation (23) and Figure 1), which is too shallow to explain a relatively sharp steepening to $L_{\rm bol} \propto t^{-3}$.

A change in the light-curve slope could occur at times $t > t_{\rm max}$ when the statistical distribution of isotopes cuts off and one or a small number of decays start to dominate the underlying radioactive power. The steeper heating evolution of Equation (36) then applies. Nuclear reaction networks for various outflow conditions do show eventual deviation from a power law (Rosswog et al. 2018), although this transition typically occurs at later times, $t \gtrsim 15$ days.

Another plausible explanation of the light-curve steepening of AT2017gfo is that some significant portion of the ejecta remained optically thick to photons for $t \approx 7$ days. As the kilonova ejecta become translucent, trapped radiation is released, causing the light curve to decline more steeply than the instantaneous heating rate. This behavior is familiar from observations of supernova light curves, which show a sharp decline from peak followed by a shallower radioactive "tail."

We illustrate the effect with a simple analytic model in Figure 4, which captures the bolometric behavior seen in detailed radiation transport calculations (e.g., Kasen et al. 2017; Kilpatrick et al. 2017; Tanaka et al. 2018; Wollaeger et al. 2018). For a kilonova to remain optically thick over $\sim$7 days requires a high opacity presumably provided by complex lanthanide ions, suggesting that GW170817 synthesized a significant mass of heavy ($A \gtrsim 130$) r-process ejecta (Kasen et al. 2013). This is consistent with the red colors observed at the later epochs, which are defining signature of lanthanide production (Barnes & Kasen 2013; Tanaka & Hotokezaka 2013).

The analytic results derived here provide workable estimates for analyzing and understanding kilonova light curves, but quantitative accuracy requires explicit thermalization transport calculations based on detailed nuclear inputs. We confirmed that the first term in Equation (51), representing electron thermalization, does a reasonable job of reproducing the detailed numerical results of Barnes et al. (2016) when $n \approx 1.2$–1.4. The second term describing the gamma-ray thermalization efficiency, however, did a poorer job, suggesting that a more sophisticated analysis of gamma-ray transport and energy deposition may be needed to analytically capture the time evolution of f_γ. In addition, alpha decay and fission are generally more efficiently thermalized than beta-decay energy and may become significant at late times, in some cases dominating the heating. Quantitative analyses of kilonova observations will require further nuclear experiment and theory to determine the detailed nucleosynthesis and decay chains of r-process nuclei.

While the results presented here clarify some aspects of the bolometric emission of kilonovae, the predicted late time colors and spectra remain rather uncertain. Once the ejecta have become fully transparent (the "nebular phase") deviations from local thermodynamic equilibrium become significant. At these phases, nonthermal beta-decay electrons will play a dominant role in setting the ionization/excitation state of the ejecta. The deposited energy may not strictly speaking be "thermalized"; nevertheless, it will presumably be radiated rapidly via some series of optical/infrared atomic transitions. Although the microscopic processes will be complex in detail, the simple estimates of the bolometric luminosity presented here are likely to remain robust.

We thank E. Waxman, E. Ofek, M. Coughlin, A. Jerkstrand, and the anonymous referee for helpful discussion and comments. This work was supported in part by the Department of Energy Office of Nuclear Physics grants DE-SC0018297 and DE-SC0017616, and by the Director, Office of Energy Research, Office of High Energy and Nuclear Physics, Divisions of Nuclear Physics, of the U.S. Department of Energy under Contract No. DE-AC02-05CH11231. J.B. is supported by the National Aeronautics and Space Administration (NASA) through the Einstein Fellowship Program, grant number PF7-180162.

ORCID iDs

Jennifer Barnes https://orcid.org/0000-0003-3340-4784

References

Abbott, B. P., Abbott, R., Abbott, T. D., et al. 2017a, PhRvL, 119, 161101
Abbott, B. P., Abbott, R., Abbott, T. D., et al. 2017b, ApJL, 848, L12
Arcavi, I. 2018, ApJL, 855, L23
Arcavi, I., Hosseinzadeh, G., Howell, D. A., et al. 2017, Natur, 551, 64
Arnett, W. D. 1982, ApJ, 253, 785
Barnes, J., & Kasen, D. 2013, ApJ, 775, 18
Barnes, J., Kasen, D., Wu, M.-R., & Martínez-Pinedo, G. 2016, ApJ, 829, 110
Chornock, R., Berger, E., Kasen, D., et al. 2017, ApJL, 848, L19
Colgate, S. A., & White, R. H. 1966, ApJ, 143, 626
Coughlin, M. W., Dietrich, T., & Doctor, Z. 2018, arXiv:1805.09371
Coulter, D. A., Foley, R. J., Kilpatrick, C. D., et al. 2017, Sci, 358, 1556
Cowperthwaite, P. S., Berger, E., Villar, V. A., et al. 2017, ApJL, 848, L17
Drout, M. R., Piro, A. L., Shappee, B. J., et al. 2017, Sci, 358, 1570
Eichler, D., Livio, M., Piran, T., & Schramm, D. N. 1989, Natur, 340, 126
Freiburghaus, C., Rosswog, S., & Thielemann, F. 1999, ApJL, 525, L121
Hotokezaka, K., Wanajo, S., Tanaka, M., et al. 2016, MNRAS, 459, 35
Kasen, D., Badnell, N. R., & Barnes, J. 2013, ApJ, 774, 25
Kasen, D., & Bildsten, L. 2010, ApJ, 717, 245
Kasen, D., Metzger, B., Barnes, J., Quataert, E., & Ramirez-Ruiz, E. 2017, Natur, 551, 80
Kasliwal, M. M., Nakar, E., Singer, L. P., et al. 2017, Sci, 358, 1559
Kilpatrick, C. D., Foley, R. J., Kasen, D., et al. 2017, Sci, 358, 1583
Lattimer, J. M., & Schramm, D. N. 1976, ApJ, 210, 549
Li, L., & Paczyński, B. 1998, ApJL, 507, L59
Lippuner, J., & Roberts, L. F. 2015, ApJ, 815, 82
McCully, C., Hiramatsu, D., Howell, D. A., et al. 2017, ApJL, 848, L32
Mendoza-Temis, J. d. J., Wu, M.-R., Langanke, K., et al. 2015, PhRvC, 92, 055805
Metzger, B. D., Martínez-Pinedo, G., Darbha, S., et al. 2010, MNRAS, 406, 2650
Meyer, B. S. 1989, ApJ, 343, 254
Nicholl, M., Berger, E., Kasen, D., et al. 2017, ApJL, 848, L18
Roberts, L. F., Kasen, D., Lee, W. H., & Ramirez-Ruiz, E. 2011, ApJL, 736, L21
Rosswog, S., Liebendörfer, M., Thielemann, F.-K., et al. 1999, A&A, 341, 499
Rosswog, S., Sollerman, J., Feindt, U., et al. 2018, A&A, 615, 132
Shappee, B. J., Simon, J. D., Drout, M. R., et al. 2017, Sci, 358, 1574
Smartt, S. J., Chen, T.-W., Jerkstrand, A., et al. 2017, Natur, 551, 75
Soares-Santos, M., Holz, D. E., Annis, J., et al. 2017, ApJL, 848, L16
Swartz, D. A., Sutherland, P. G., & Harkness, R. P. 1995, ApJ, 446, 766
Tanaka, M., & Hotokezaka, K. 2013, ApJ, 775, 113
Tanaka, M., Kato, D., Gaigalas, G., et al. 2018, ApJ, 852, 109
Tanaka, M., Utsumi, Y., Mazzali, P. A., et al. 2017, PASJ, 69, 102
Tanvir, N. R., Levan, A. J., González-Fernández, C., et al. 2017, ApJL, 848, L27
Waxman, E., Ofek, E., Kushnir, D., & Gal-Yam, A. 2018, MNRAS, 481, 3423
Wollaeger, R. T., Korobkin, O., Fontes, C. J., et al. 2018, MNRAS, 478, 3298